

A Direct Method for Photoacoustic Tomography with Inhomogeneous Sound Speed

Zakaria Belhachmi ^{*} Thomas Glatz [†] Otmar Scherzer [‡]

November 29, 2021

Abstract

The standard approach for photoacoustic imaging with variable speed of sound is *time reversal*, which consists in solving a well-posed final-boundary value problem backwards in time. This paper investigates the iterative Landweber regularization algorithm, where convergence is guaranteed by standard regularization theory, notably also in cases of *trapping* sound speed or for short measurement times. We formulate and solve the direct and inverse problem on Ω , what is common in standard photoacoustic imaging, but not for time-reversal algorithms, Ω^* . We both the direct and adjoint photoacoustic operator an interior and an exterior equation Ω^* . The prior is solved using a Galerkin scheme in space and finite difference discretization in time, while the latter boundary integral equation. We therefore use a BEM-FEM approach for numerical solution of the forward operators. We analyze this method, prove convergence, and provide numerical tests. Moreover, we compare the approach to time reversal.

Keywords: Photoacoustic Imaging, Variable Sound Speed, Regularization

Introduction

Photoacoustic Imaging (PAI) is a novel imaging technique that allows for three dimensional imaging of small biological or medical specimens with high spatial resolution. It utilizes that an object expands and emits ultrasound waves when it is exposed to a short pulse of electromagnetic radiation (see e.g. [43, 40]). The emitted ultrasound is assumed to be proportional to the electromagnetic *absorption density* which provides detailed anatomical and functional information. PAI aims for visualization of the absorption density by using measurements of the emitted wave outside of the object.

Opposed to the standard PAI problem [24, 39, 40] we assume a spatially varying speed of sound. The underlying mathematical model of the wave propagation with

^{*}Laboratoire de Mathématiques LMIA, Université de Haute Alsace, 4, rue des Frères Lumière, 68200 Mulhouse, France. (zakaria.belhachmi@uha.fr)

[†]Computational Science Center, University of Vienna, Oskar-Morgenstern Platz 1, A-1090 Vienna, Austria. (thomas.glatzl@univie.ac.at)

[‡]Computational Science Center, University of Vienna, Oskar-Morgenstern Platz 1, A-1090 Vienna, Austria, and Johann Radon Institute for Computational and Applied Mathematics (RICAM), Austrian Academy of Sciences, Altenbergerstraße 69, A-4040 Linz, Austria. (otmar.scherzer@univie.ac.at)

spatially varying sound speed $c(x)$ is the *acoustic wave equation*

$$\begin{aligned} \frac{1}{c^2(x)}y''(x,t) - \Delta y(x,t) &= 0 \text{ in } \mathbb{R}^n \times (0, \infty), \\ y(x,0) &= f(x) \text{ in } \mathbb{R}^n, \\ y'(x,0) &= 0 \text{ in } \mathbb{R}^n \end{aligned} \tag{1}$$

where f denotes the absorption density, which is proportional to the absorbed electromagnetic energy.

The *inverse problem* of photoacoustics with variable wave speed consists in determining the function f from measurement data m of y on a surface $\partial\Omega$ over time $(0, T)$. That is, it consists in solving the equation

$$y|_{\Sigma} = m. \tag{2}$$

With constant sound speed there exists a variety of analytical reconstruction formulas and numerical inversion techniques. We mention [45, 44, 42, 41, 46], see also the surveys [24, 40, 25, 38]. In the case of inhomogeneous sound speed, exact reconstruction formulas have been derived in [3]. A numerical method, providing approximations, is *time reversal* [13, 17, 16, 21], . Thereby the measurement data serve as Dirichlet boundary data, and the *initial* conditions at final observation time T are assumed to be identically zero. On top of the original algorithm of Fink [13], the approach in [35] suggests a harmonic extension of the boundary data at time T as initialization data. The reconstruction obtained by time-reversal, lets say f_T , approximates the true solution f as T increases to infinity. The exact f can be reconstructed if $y(\cdot, T) \equiv 0$, which happens, aside from trivial cases, only in odd dimensions and for homogeneous sound speed. In all other cases the results are error-prone. Moreover, this method produces approximations of f only under *non-trapping* conditions on c (see [21, 20]).

Stefanov and Uhlmann [35] showed that if $\text{diam}(\Omega) = 2T_0$ (where $\text{diam}(\Omega)$ denotes the diameter of Ω with respect to the Riemannian metric $c^{-2}dx$), then an observation time $T > T_0$ is sufficient for a unique reconstruction of f . However, for stability of the inverse problem one needs longer measurement times and a non-trapping speed of sound condition. In fact, if the measurement time T is larger than a certain threshold, depending on the longest geodesic in the metric induced by c , the algorithm presented in [35] provides a theoretically exact reconstruction in terms of a Neumann series that contains multiple, subsequent time reversal and forward propagation of the data term. A computational realization of this approach has been investigated in [32]. This algorithm serves as a benchmark for our proposed algorithm.

The presented approach for PAI inversion with variable sound speed relies on linear regularization theory [15]. Specifically, we obtain regularized convergence to the *minimum norm solution* even for short measurement times. Moreover, we obtain a new reconstruction method that does not require an artificial cut-off of the measurement data, nor harmonic extension of the data at the final observation time T .

For the numerical computations, we decouple the wave equation into an interior part (solved by finite element methods), and an exterior part (with homogeneous sound speed) that is rewritten in terms of a boundary integral formulation. We then solve the coupled BEM-FEM system numerically. Note that by this approach we use exact, non-reflecting boundary conditions [1, 11] and therefore avoid the necessity of a *perfectly matched layer* to deal with the cut-off outside the domain of interest. The results are compared to conventional time reversal and the Neumann-series approach.

The paper is organized as follows: In Section 1 we formulate the direct photoacoustic operator L in a suitable choice of function spaces, and derive the adjoint. In Section 2 we give a short overview about Landweber iteration and review some regularization results regarding convergence and convergence rates in view of PAI reconstruction. Moreover, we discuss the relation to the Neumann series approach in [35]. In Section 3, we formulate the transmission problem for the wave equation used for numerical computation of both the direct and the adjoint problem. We state the boundary relations used for taking into account the exterior domain. In addition, we briefly describe the used discretization. Finally, Section 4 provides a comparison of our reconstruction algorithm with the state-of-the-art reconstruction by time reversal and the *enhanced* time reversal Neumann series method from [35].

All along this paper we use the following notation and abbreviations:

Notation 1 *Let Ω be a non-empty, open, bounded and connected domain in \mathbb{R}^n with C^1 -boundary $\partial\Omega$. The vector $\mathbf{n}(x)$, with $x \in \partial\Omega$, denotes the outward pointing unit normal vector. We use the following sets*

$$\Omega^+ := \mathbb{R}^n \setminus \overline{\Omega}, \quad \Omega^- := \Omega \quad \text{and} \quad \Sigma := \partial\Omega \times (0, T) .$$

We use the following Hilbert spaces:

- $L^2(\Omega) = \{\rho \in L^2(\mathbb{R}^n) : \rho \equiv 0 \text{ in } \mathbb{R}^n \setminus \Omega\}$, with inner product

$$\langle \rho_1, \rho_2 \rangle_{L^2(\Omega)} = \int_{\mathbb{R}^n} \rho_1(x) \rho_2(x) dx .$$

- For $\hat{\Omega} = \Omega$ or \mathbb{R}^n :

- Let $H_0^1(\hat{\Omega})$ be the closure of differentiable functions on \mathbb{R}^n with compact support in $\hat{\Omega}$, associated with the inner product

$$\langle \rho_1, \rho_2 \rangle_{H_0^1(\hat{\Omega})} = \int_{\mathbb{R}^n} \nabla \rho_1(x) \cdot \nabla \rho_2(x) dx .$$

- $H^1(\hat{\Omega})$ denotes the standard Sobolev space with inner product

$$\langle \rho_1, \rho_2 \rangle_{H^1(\hat{\Omega})} = \int_{\hat{\Omega}} \rho_1(x) \rho_2(x) + \nabla \rho_1(x) \cdot \nabla \rho_2(x) dx .$$

- $L^2(\partial\Omega)$ denotes the standard Hilbert space of square integrable functions on $\partial\Omega$ with inner product

$$\langle \phi_1, \phi_2 \rangle_{L^2(\partial\Omega)} = \int_{\partial\Omega} \phi_1(x) \phi_2(x) dS(x) .$$

$L^2(\Sigma)$ denotes the standard Hilbert space of square integrable functions on Σ with inner product

$$\langle \phi_1, \phi_2 \rangle_{L^2(\Sigma)} = \int_0^T \int_{\partial\Omega} \phi_1(x, t) \phi_2(x, t) dS(x) dt .$$

- The induced norms are denoted by $\|\cdot\|_{L^2(\Omega)}$, $\|\cdot\|_{L^2(\Sigma)}$, $\|\cdot\|_{H^1(\hat{\Omega})}$ and $\|\cdot\|_{H_0^1(\hat{\Omega})}$, respectively.

For Ω bounded, on $H_0^1(\Omega)$, the norms $\|\cdot\|_{H_0^1(\Omega)}$ and $\|\cdot\|_{H^1(\Omega)}$ are equivalent (see [2, Theorem 6.28]):

$$C_0 \|\rho\|_{H^1(\Omega)} \leq \|\rho\|_{H_0^1(\Omega)} \leq \|\rho\|_{H^1(\Omega)} \quad \text{for all } \rho \in H_0^1(\Omega). \quad (3)$$

- The trace operator $\gamma_\Omega : H^1(\mathbb{R}^n) \rightarrow L^2(\partial\Omega)$ restricts functions defined on \mathbb{R}^n onto $\partial\Omega$, respectively. This operator is the decomposition of the standard trace operator

$$\gamma : H^1(\Omega) \rightarrow L^2(\partial\Omega)$$

and the restriction operator

$$R : H^1(\mathbb{R}^n) \rightarrow H^1(\Omega),$$

and thus as a composition of two bounded operators [2, Theorem 5.22] bounded. We abbreviate the norm with

$$\mathcal{C}_\gamma := \|\gamma \circ R\|. \quad (4)$$

Notation 2 The absorption density f and the sound speed c^2 are supposed to satisfy:

- $c \in C^1(\bar{\Omega})$, satisfies $0 < c_{\min} \leq c(x) \leq c_{\max}$ and c is non-constant in Ω .
- Without loss of generality we assume that $c \equiv 1$ in Ω^+ .
- The absorption density function $f \in H_0^1(\Omega)$ is compactly supported in Ω : $\text{supp}(f) \subseteq \Omega$.

For the sake of simplicity of notation we omit space and time arguments of functions whenever this is convenient.

1 Direct Problem of Wave-Propagation

We analyze the *wave operator* L mapping the absorption density f onto the solution y of the wave equation (1) restricted to Σ . That is

$$L : H_0^1(\Omega) \rightarrow L^2(\Sigma), \quad f \mapsto y|_\Sigma. \quad (5)$$

In the following we show that L is bounded. Let us write

$$E(t) := \int_{\mathbb{R}^n} \frac{1}{c^2} (y')^2 + |\nabla y|^2 dx. \quad (6)$$

Computing the derivative of E with respect to t and taking into account (1) gives

$$E'(t) = 2 \int_{\mathbb{R}^n} \frac{1}{c^2} y'' y' - \Delta y y' dx = 0.$$

Consequently

$$E(t) = E(0) = \|f\|_{H_0^1(\Omega)}^2, \quad (7)$$

which implies that

$$\frac{1}{c^2} \int_{\mathbf{R}^n} (y')^2 dx \leq \int_{\mathbf{R}^n} \frac{1}{c^2} (y')^2 dx \leq \|f\|_{H_0^1(\Omega)}^2 \quad (8)$$

and

$$\|y(t)\|_{H_0^1(\mathbf{R}^n)} \leq \|f\|_{H_0^1(\Omega)} \quad (9)$$

for every $t \in (0, T)$.

Lemma 1.1 *Let y be the solution of (1), then*

$$\|y(t)\|_{H^1(\mathbf{R}^n)} \leq \mathcal{C}(T) \|f\|_{H_0^1(\Omega)}, \quad \text{for all } t \in (0, T). \quad (10)$$

with

$$\mathcal{C}(T) := \sqrt{C_0},$$

where C_0 is defined in (3).

Proof. First, we note that for arbitrary $t \in (0, T)$, it follows from (8) that:

$$\begin{aligned} \int_{\mathbf{R}^n} (y(x, t) - y(x, 0))^2 dx &= \int_{\mathbf{R}^n} \left(\int_0^t y'(x, \hat{t}) d\hat{t} \right)^2 dx \\ &\leq t \int_{\mathbf{R}^n} \int_0^t (y'(x, \hat{t}))^2 d\hat{t} dx \\ &= t \int_0^t \int_{\mathbf{R}^n} (y'(x, \hat{t}))^2 dx d\hat{t} \\ &\leq t^2 \|f\|_{H_0^1(\Omega)}^2 \\ &\leq T^2 \|f\|_{H_0^1(\Omega)}^2. \end{aligned}$$

Because $(a - b)^2 \geq \frac{1}{2}a^2 - b^2$ it follows from (3) that

$$\begin{aligned} \int_{\mathbf{R}^n} (y(x, t))^2 dx &\leq 2 \int_{\mathbf{R}^n} (y(x, t) - y(x, 0))^2 dx + 2 \int_{\mathbf{R}^n} (y(x, 0))^2 dx \\ &\leq 2T^2 \|f\|_{H_0^1(\Omega)}^2 + 2 \|f\|_{L^2(\Omega)}^2 \\ &\leq 2 \max\{1, T^2\} \|f\|_{H^1(\Omega)}^2. \end{aligned}$$

Because $f \in H_0^1(\Omega)$ it follows that

$$\|y(t)\|_{L^2(\mathbf{R}^n)}^2 \leq \frac{2}{C_0} \max\{1, T^2\} \|f\|_{H_0^1(\Omega)}^2.$$

This, together with (9) shows that for all $t \in (0, T)$:

$$\|y(t)\|_{H^1(\mathbf{R}^n)} \leq \sqrt{C_0} \|f\|_{H_0^1(\Omega)}.$$

□

In the following we prove boundedness of L :

Theorem 1.2 *The operator $L : H_0^1(\Omega) \rightarrow L^2(\Sigma)$ is bounded and*

$$\|L\| \leq \mathcal{C}_\gamma \mathcal{C}(T) \sqrt{T}. \quad (11)$$

Proof. For given f let y be the solution of (1). From (6) it follows that the solution y of (10) is in $H^1(\mathbb{R}^n)$ for every $t > 0$. Thus from (4) and (10) it follows that

$$\|y\|_\Sigma^2 = \int_0^T \int_{\partial\Omega} y^2(t) \, d\sigma dt \leq \mathcal{C}_\gamma^2 \int_0^T \|y(t)\|_{H^1(\mathbb{R}^n)}^2 \, dt \leq \mathcal{C}_\gamma^2 \mathcal{C}(T)^2 T \|f\|_{H_0^1(\Omega)}^2,$$

which gives the assertion.

Remark 1.3 (Injectivity of L) *In order to obtain injectivity of L , we need T to be sufficiently large. To specify this, we define*

$$T_0 := \max_{x \in \Omega} (\text{dist}(x, \partial\Omega)), \quad (12)$$

where $\text{dist}(x, \partial\Omega)$ is the distance of x to the closest point $x' \in \partial\Omega$ with respect to the Riemannian metric $c^{-2}dx$ (see also [32]). From [35, Thm. 2] it follows that if $T > T_0$, then $L[f] = 0$ implies $f = 0$ in $(0, T) \times \mathbb{R}^n$.

□

In the following we characterize the adjoint of $L : H_0^1(\Omega) \rightarrow L^2(\Sigma)$ on a dense subset of $L^2(\Sigma)$. Because we know from elementary functional analysis that $L^* : L^2(\Sigma) \rightarrow H_0^1(\Omega)$ is bounded,

Definition 1.4 *Let i be the embedding operator from $H_0^1(\Omega)$ to $L^2(\Omega)$. Then $i^* : L^2(\Omega) \rightarrow H_0^1(\Omega)$ is the operator which maps a function $\psi \in L^2(\Omega)$ onto the solution of the equation*

$$-\Delta u = \psi \text{ in } \Omega, \quad u = 0 \text{ on } \partial\Omega.$$

That is

$$i^* = -\Delta^{-1}, \quad (13)$$

where Δ is the Laplace-operator with homogeneous Dirichlet boundary conditions.

In the following we derive the adjoint L^* of the operator L , which is required for the implementation of the Landweber iteration below.

Theorem 1.5 *For $h \in C^\infty((0, T) \times \partial\Omega)$ the adjoint of the operator L , defined in (5), is given by*

$$L^*[h] = i^* \circ L_D^*[h] \quad (14)$$

where

$$L_D^*[h] = \frac{1}{c^2} z'(0) \Big|_\Omega, \quad (15)$$

and $z := z(h)$ is the weak solution of

$$\begin{aligned} \frac{1}{c^2} z'' - \Delta z &= 0 \text{ in } \mathbb{R}^n \setminus \partial\Omega \times (0, T), \\ z(T) = z'(T) &= 0 \text{ in } \mathbb{R}^n, \\ [z] = 0, \quad \left[\frac{\partial z}{\partial \mathbf{n}} \right] &= h \text{ on } \partial\Omega \times (0, T). \end{aligned} \quad (16)$$

Here

$$[z] := z^+|_{\Sigma} - z^-|_{\Sigma} \text{ and } \left[\frac{\partial z}{\partial \mathbf{n}} \right] := \frac{\partial z^+}{\partial \mathbf{n}} \Big|_{\Sigma} - \frac{\partial z^-}{\partial \mathbf{n}} \Big|_{\Sigma}$$

where $z^+ := z|_{\Omega^+ \times (0, T)}$ and $z^- := z|_{\Omega^- \times (0, T)}$.

Proof. For $h \in C^\infty((0, T) \times \partial\Omega)$ the existence of a weak solution of (42) is proven in the Appendix. Taking $v = y$ where y denotes the solution of (1) it follows that

$$\begin{aligned} \int_{\Sigma} hL[f] dS(x)dt &= \int_{\Sigma} hy dS(x)dt \\ &= \int_{\Omega} \frac{z'(0)}{c^2} f dx \\ &= \int_{\Omega} \Delta \left[\Delta^{-1} \left[\frac{z'(0)}{c^2} \right] \right] f dx \\ &= - \int_{\Omega} \nabla \left(\Delta^{-1} \left[\frac{z'(0)}{c^2} \right] \right) \cdot \nabla f dx \\ &= \int_{\Omega} \nabla i^* \left[\frac{z'(0)}{c^2} \right] \cdot \nabla f dx \\ &= \left\langle i^* \left[\frac{z'(0)}{c^2} \right], f \right\rangle_{H_0^1(\Omega)}. \end{aligned} \tag{17}$$

□

2 Landweber Iteration for Solving the Inverse Problem of Photoacoustics

The *photoacoustic imaging problem* rewrites as the solution of the operator equation:

$$L[f] = m. \tag{18}$$

If the null-space of L is non-trivial, then iterative regularization algorithms, in general, when m is an element of the range of L reconstruct the *minimum norm solution*

$$f^\dagger = L^\dagger[m], \tag{19}$$

where L^\dagger denotes the Moore-Penrose inverse of L (see [31] for a survey on Moore-Penrose inverses).

We propose to use the Landweber's iteration for solving (18), because it can be compared with time reversal methods, which are the standard references in this field. More efficient regularization algorithms are at hand [19], but these are less intuitive to be compared with time reversal.

In the following we review properties of the Landweber iteration in an abstract setting (see [15, 9]). We use the same notation for the abstract operator and the photoacoustic operator and measurement data m , m^δ , respectively, in order to have direct connection.

2.1 Abstract Landweber Regularization

Everything that is formulated below is based on the following assumption:

Assumption 2.1 Let $L : H_1 \rightarrow H_2$ be an operator between Hilbert spaces H_1 and H_2 satisfying $\omega \|L\|^2 \leq 1$ for some $\omega > 0$. Moreover, we assume that data m^δ of m is available (typically considered as noisy data), which satisfy

$$\|m - m^\delta\|_{H_2} \leq \delta. \quad (20)$$

Then the Landweber iteration reads as follows:

$$f_0 := 0 \quad \text{and} \quad f_k^\delta = f_{k-1}^\delta - \omega L^* [L[f_{k-1}^\delta] - m^\delta], \quad k = 1, 2, \dots \quad (21)$$

In case $\delta = 0$, that is, if $m^\delta = m$, then we write f_k instead of f_k^δ .

Let $\tau > 1$ be some fixed constant. The Landweber iteration is only iterated for $k = 1, 2, \dots$ as long as

$$\|m^\delta - L[f_k^\delta]\|_{H_2} > \tau\delta. \quad (22)$$

The index, where (22) is violated for the first time is denoted by $k_*(\delta, m^\delta)$.

The following theorem shows that the Landweber iteration converges to the best-approximating solution:

Theorem 2.2 Let $m \in \mathcal{R}(L)$ (note that the range of L equals the domain of L^\dagger).

- Let $\delta = 0$, then the Landweber iterates (f_k) (cf. (21)) converge to the f^\dagger , i.e., $\|f_k - f^\dagger\|_{H_1} \rightarrow 0$. In addition, we have the series expansion:

$$f^\dagger = \sum_{j=0}^{\infty} (I - \omega L^* L)^j [L^*[m]].$$

- For $\delta > 0$ and m^δ satisfying $\|m - m^\delta\|_{H_2} \leq \delta$ let $k_*^\delta = k_*(\delta, m^\delta)$ as in (22). Then

$$f_{k_*^\delta}^\delta \rightarrow_{H_1} f^\dagger.$$

Moreover, if $m \notin \mathcal{D}(L^\dagger)$, then $\|f_k\|_{H_1} \rightarrow \infty$ as $k \rightarrow \infty$.

In the following we prove properties of the wave-operator L , such that we can apply the general regularization results.

2.2 Convergence of the Landweber Iteration for the Photoacoustic Problem

In the following we apply Theorem 2.2, for the photoacoustic imaging problem.

Corollary 2.3 Let $\omega \leq \frac{1}{c_2^2 c^2(T)T} = \mathcal{O}(1/T^3)$ and $L : H_0^1(\Omega) \rightarrow L^2(\Sigma)$ as in (5). Moreover, assume that

$$\|m - m^\delta\|_{L^2(\Sigma)} \leq \delta.$$

Then the Landweber iterates satisfy:

- If $\delta = 0$, then

$$f^\dagger = \sum_{k=0}^{\infty} (I - L^* L)^k [L^*[m]].$$

- For $\delta > 0$, the Landweber iteration is terminated at $k_*(\delta) := k_*(\delta, m^\delta)$ according to (22). Then

$$f_{k_*^\delta}^\delta \rightarrow f^\dagger \text{ for } \delta \rightarrow 0.$$

- If $T > T_0$, the reconstruction is unique, and $f_{k_*(\delta)}^\delta$ converges to the unique solution.

Proof. First, we note that from (11) it follows that $\omega \|L\|^2 \leq 1$. Then, the first two items follow directly from Theorems 2.2.

From the injectivity of L for $T > T_0$ (see Remark 1.3) it follows that $f^\dagger = f$, which implies unique reconstruction. \square

2.3 Comparison with Time Reversal

We compare our approach with different variants of *time reversal*. We formally define the time reversal operator:

$$\bar{L}[h] = z(\cdot, 0), \tag{23}$$

where z is a solution of

$$\begin{aligned} \frac{1}{c^2} z'' - \Delta z &= 0 \text{ in } \Omega \times (0, T), \\ z(T) = z'(T) &= 0 \text{ in } \Omega, \\ z &= h \text{ on } \partial\Omega \times (0, T), \end{aligned} \tag{24}$$

The fundamental differences between \bar{L} and L^* are that \bar{L} is defined for functions with support in Ω and that therefore L^* requires a transmission condition in its definition.

Stefanov and Uhlmann [35] modified the time reversal approach in the following sense: Rather than assuming (in most cases unjustified) the initial data $z(T) \equiv 0$, they used the harmonic extension of the data term $h(s, T)$, for $s \in \partial\Omega$, as initial datum at T . That is, for

$$-\Delta\phi = 0 \text{ in } \Omega, \text{ with } \phi(\cdot) = m(\cdot, T) \text{ on } \partial\Omega$$

the modified time-reversal operator

$$\tilde{\tilde{L}}[h] = z(\cdot, 0) \tag{25}$$

is defined by the solution of equation

$$\begin{aligned} \frac{1}{c^2} z'' - \Delta z &= 0 \text{ in } \Omega \times (0, T), \\ z(T) = \phi, \quad z'(T) &= 0 \text{ in } \Omega, \\ z &= h \text{ on } \partial\Omega \times (0, T). \end{aligned} \tag{26}$$

They were able to show that under non-trapping conditions and for sufficiently large measurement time T , there exists a compact operator $K : H_0^1(\Omega) \rightarrow H_0^1(\Omega)$ satisfying $\|K\| < 1$, and

$$\tilde{\tilde{L}}L = Id - K, \tag{27}$$

Therefore, the initial condition f can be expanded into the Neumann series

$$f = \sum_{j=0}^{\infty} K^j[m]. \quad (28)$$

By induction, it is easy to see that the m -th iterate can be written as

$$f_k = f_{k-1} - \tilde{L}[L[f_{k-1}] - m], \quad (29)$$

where

$$f_k = \sum_{j=0}^{\infty} K^j[m].$$

At this point, we emphasize on the structural similarity between (29) and (21).

Remark 2.4 *We emphasize that for time-reversal there is no theory on stopping in case of error-prone data, such as we have available for the Landweber iteration.*

3 Numerical realization of L and L^*

We solve (1) and (16) with the same numerical framework. By changing the variable $t \rightarrow T - t$ in (16), both equations can be rewritten as the transmission problem:

$$\begin{aligned} \frac{1}{c^2}v'' - \Delta v &= 0 && \text{in } \mathbb{R}^n \setminus \partial\Omega \times (0, T), \\ v(0) = v_0, \quad v'(0) &= 0 && \text{in } \mathbb{R}^n \setminus \partial\Omega, \\ \left[\frac{\partial v}{\partial \mathbf{n}} \right] &= \rho, \quad [v] = 0 && \text{on } \Sigma. \end{aligned} \quad (30)$$

where for (1) $\rho \equiv 0$ and $v_0 = f \in H_0^1(\Omega)$ and for (16) we have $\rho \equiv h \in L^2(\Sigma)$ and $v_0 \equiv 0$.

Let $v_0^- = v_0$ in Ω^- , $v_0^+ = 0$ in Ω^+ , then $v^\pm = v|_{\Omega^\pm}$ satisfy, respectively:

$$\begin{aligned} \frac{1}{c^2}v_\pm'' - \Delta v_\pm &= 0 && \text{in } \Omega^\pm \times (0, T), \\ v_\pm(0) = v_0^\pm, \quad v_\pm'(0) &= 0 && \text{in } \Omega^\pm, \end{aligned} \quad (31)$$

together with the transmission conditions

$$\left[\frac{\partial v}{\partial \mathbf{n}} \right] = \rho \text{ and } [v] = 0 \quad \text{on } \Sigma. \quad (32)$$

Let G denote the fundamental solution of the standard wave equation with $c^2 \equiv 1$ in \mathbb{R}^n . It is defined in $\mathbb{R}^n \times \mathbb{R}$, and its explicit expression

$$G(x, t) = \begin{cases} \frac{H(t-|x|)}{2\pi\sqrt{t^2-|x|^2}}, & n = 2, \\ \frac{\delta(t-|x|)}{4\pi|x|}, & n = 3, \end{cases}$$

with H denoting the Heaviside step function, and $\delta(\cdot)$ being the 3D Dirac delta distribution (see, e.g., [14]).

The (retarded) single- and double- layer potentials for $(x, t) \in \Sigma$ are defined by

$$\begin{aligned}\mathcal{V}[\varphi](x, t) &:= \int_0^t \int_{\partial\Omega} G(y-x, t-\tau) \varphi(y, \tau) dS_y d\tau, \\ \mathcal{K}[\psi](x, t) &:= \int_0^t \int_{\partial\Omega} \frac{\partial G(y-x, t-\tau)}{\partial \mathbf{n}} \psi(y, \tau) dS_y d\tau.\end{aligned}\tag{33}$$

Because we assume that $c = 1$ outside of Ω and because we assume that $\partial\Omega$ is a C^1 boundary, it follows that v^+ satisfies (see [18]):

$$\frac{1}{2}v^+(x, t) = -\mathcal{V}\left[\frac{\partial v^+}{\partial \mathbf{n}}\right](x, t) - \mathcal{K}[v^+](x, t), \quad \text{for all } (x, t) \in \Sigma.\tag{34}$$

The transmission conditions imply that

$$v^+ = v^- \quad \text{and} \quad \frac{\partial v^+}{\partial \mathbf{n}} = \frac{\partial v^-}{\partial \mathbf{n}} + \rho \quad \text{on } \Sigma.$$

Therefore the equation for $v = v^-$ on $\Omega = \Omega^-$ can be rewritten as follows:

$$\begin{aligned}\frac{1}{c^2}v'' - \Delta v &= 0 && \text{in } (\Omega) \times (0, T), \\ v(0) = v_0, \quad v'(0) &= 0 && \text{in } \Omega, \\ \frac{1}{2}v + \mathcal{V}\left[\frac{\partial v}{\partial \mathbf{n}} + \rho\right] + \mathcal{K}[v] &= 0 && \text{on } \Sigma.\end{aligned}\tag{35}$$

The numerical solution is based on a weak formulation of (35). Integrating over Ω , multiplying by $w \in H^1(\Omega)$ and integration by parts of the first line of (35) gives

$$\frac{d^2}{dt^2} \left\langle \frac{1}{c^2}v(t), w \right\rangle_{L^2(\Omega)} + \langle \nabla v(t), \nabla w \rangle_{L^2(\Omega)} - \left\langle \frac{\partial v}{\partial \mathbf{n}}(t), w \right\rangle_{L^2(\partial\Omega)} = 0.$$

Additionally we introduce the unknown function $\lambda := \frac{\partial v}{\partial \mathbf{n}}$ defined on Σ . We are therefore searching for a solution $(v, \lambda) \in H^1(\Omega) \times H^{-1/2}(\partial\Omega)$ that satisfies for almost all $t \in (0, T)$ the system

$$\begin{aligned}\frac{d^2}{dt^2} \left\langle \frac{1}{c^2}v(t), w \right\rangle_{L^2(\Omega)} + \langle \nabla v(t), \nabla w \rangle_{L^2(\Omega)} - \langle \lambda, w \rangle_{L^2(\partial\Omega)} &= 0 && \text{for all } w \in H^1(\Omega), \\ v(0) = v_0, v'(0) &= 0 && \text{in } \Omega, \\ \frac{1}{2}v(t) + \mathcal{V}[\lambda + \rho](t) + \mathcal{K}[v](t) &= 0 && \text{on } \Sigma.\end{aligned}\tag{36}$$

For detailed analysis of the discretization of equations of that type (36) we refer to [11], since we closely follow their approach.

Next, we discuss the time discretization of the integrals $\mathcal{V}[\lambda]$ and $\mathcal{K}[v]$. We consider a uniform time discretization of the interval $(0, T)$ into N steps of length $\Delta_t = T/N$, and defining the discrete time levels $t_n = n\Delta_t$. Following [12], by using Lubich's convolution quadrature formula [29], we approximate $\mathcal{V}[\lambda]$ and $\mathcal{K}[v]$ at the time steps

$t_n, n = 0, \dots, N$ by

$$\begin{aligned}\mathcal{V}[\varphi](x, t_n) &\approx \sum_{j=0}^n \int_{\partial\Omega} w_{n-j}^{\mathcal{V}}(\Delta_t, |x-y|) \varphi(y) dS_y, \\ \mathcal{K}[\psi](x, t_n) &\approx \sum_{j=0}^n \int_{\partial\Omega} w_{n-j}^{\mathcal{K}}(\Delta_t, |x-y|) \psi(y) dS_y.\end{aligned}\tag{37}$$

where the coefficients $w_n^{\mathcal{V}}$ and $w_n^{\mathcal{K}}$ satisfy

$$\begin{aligned}w_n^{\mathcal{V}}(\Delta_t, |x-y|) &= \frac{\beta}{2\pi L} \sum_{l=0}^{L-1} K^{\mathcal{V}}\left(|x-y|, \frac{\gamma(\rho \exp(il2\pi/L))}{\Delta_t}\right) \exp(-in2\pi/L), \\ w_n^{\mathcal{K}}(\Delta_t, |x-y|) &= \frac{\beta}{2\pi L} \sum_{l=0}^{L-1} K^{\mathcal{K}}\left(|x-y|, \frac{\gamma(\rho \exp(il2\pi/L))}{\Delta_t}\right) \exp(-in2\pi/L),\end{aligned}\tag{38}$$

where

$$K^{\mathcal{V}}(r, s) = K_0(rs), \quad K^{\mathcal{K}}(r, s) = -sK_1(rs) \frac{\partial r}{\partial \mathbf{n}},$$

and $K_0(\cdot), K_1(\cdot)$ are the second kind modified Bessel functions of , respectively. The function γ is given by $\gamma(z) = 3/2 - 2z + 1/2z^2$ and is the associated characteristic quotient of the used backward differentiation formula method of order two. For the involved constants we choose $L = 2N$ and $\beta = \epsilon^{1/2N}$, where ϵ is the machine precision (see [29, 12] for more details).

In the first equation in (36), the second time derivative is approximated using the second order central difference expression

$$\frac{d^2}{dt^2} v^n = \frac{1}{\Delta t^2} (v^{n+1} - 2v^n + v^{n-1}) + \mathcal{O}(\Delta t^2),$$

where $v^n := v(\cdot, t_n)$. The first time derivative occurring in the initial condition is also discretized by central differences, namely

$$\frac{d}{dt} v^0 = \frac{1}{\Delta t} (v^1 - v^{-1}) + \mathcal{O}(\Delta t^2).$$

From that we can restate the initial conditions as

$$\begin{aligned}\langle v^0, w \rangle &= \langle v^0, w \rangle, \\ \langle v^1, w \rangle &= \left\langle \frac{1}{c^2} v^0, w \right\rangle - \frac{1}{2} \Delta t^2 (\langle \nabla v^0, \nabla w \rangle \langle \lambda^0, w \rangle), \quad \text{for all } w \in H^1(\Omega).\end{aligned}\tag{39}$$

Using this, the explicit Euler discretization of (36) is stated as

$$\begin{aligned}\frac{1}{\Delta t^2} \left\langle \frac{1}{c^2} (v^{n+1} - 2v^n + v^{n-1}), w \right\rangle + \langle \nabla v^n, \nabla w \rangle - \langle \lambda^n, w \rangle &= 0, \quad \text{for all } w \in H^1(\Omega), \\ \frac{1}{2} v^{n+1}(t) + &= 0 \quad \text{on } \Sigma,\end{aligned}\tag{40}$$

for all $1 \leq n \leq N$.

In space Ω is triangulated, and we use piecewise quadratic basis functions, supplemented by one cubic function for v . The functions Λ and $v|_{\partial\Omega}$ are discretized by the use of piecewise linear functions. With this ansatz a mass-lumped integration scheme can be robustly implemented, which is not the case for purely piecewise quadratic functions. The details and numerical analysis to this scheme can be found in [6].

4 Numerical experiments and results

Here, we present numerical results for the Landweber reconstructions and compare it with standard time-reversal reconstructions and the Neumann-series-approach (28) - always computed with the same discretization. We concentrate in particular on the cases where classical time reversal techniques have their theoretical and practical drawbacks, that is, so-called *trapping speed geometries* and short measurement times. In these cases, neither time reversal nor the Neumann-series (28) provide theoretical convergence. As we have shown in Corollary 2.3, the Landweber reconstruction converges to the least squares solution, regardless of the chosen measurement time. In what follows, we also show the practical applicability of our method in such cases.

To create the data sets, we use the discretization of the coupled method introduced in Section 3. The forward computations are performed in a circle of radius 1. For both simulation and reconstructions, the chosen finite element space is that of continuous, piecewise quadratic functions in space. For the spatial discretization of the boundary terms, we take piecewise linear basis functions. Note that for convenience and to optimize the computational effort, we assume $\partial\Omega$ to be a circle of Radius R . For the time discretization, we choose the step size $\Delta t = h/(15c_{\max})$ for the simulation and $\Delta t_r = h_r/(14c_{\max})$. Here c_{\max} is the maximum speed of sound. The time reversal reconstructions are obtained by solving the initial boundary value problem (24) with homogeneous initial values. In the images, when we used the harmonic extension time-reversal (26), the heading is *Neumann*. The Landweber reconstruction is performed by the scheme described in Corollary 2.3. The choices of c in both the trapping and non-trapping case have been taken from [32].

4.1 Non-trapping sound speed

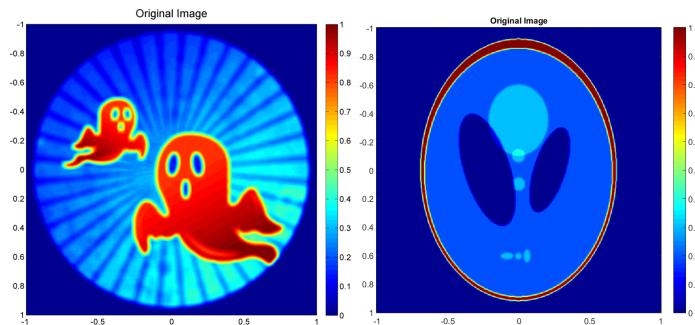


Figure 1:

Let's first consider the case of the non-trapping speed

$$c(x) = \begin{cases} 1 + 0.2 \sin(2\pi x_1) + 0.1 \cos(2\pi x_2), & x \in B_{R-\varepsilon}, \\ 1 & \text{outside } B_R. \end{cases}$$

Note that here and below, the speed of sound is smoothed out near the boundaries to satisfy our smoothness assumptions. The time reversal method already gives reliable reconstructions if the measurement time T is sufficiently large. For the test example, a measurement time of $T = 4T_0$ (see Remark 1.3) is enough to provide a quantitatively reasonable reconstruction by time reversal. This is illustrated in Figure 3. We

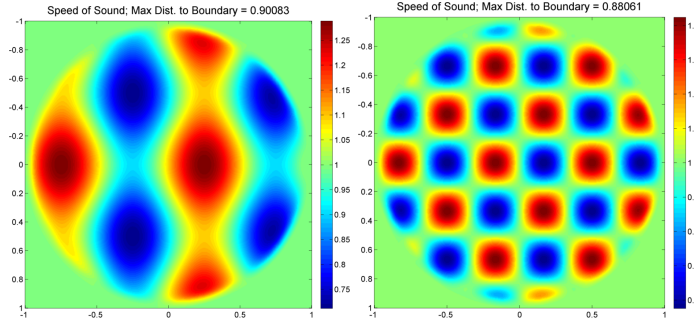


Figure 2:

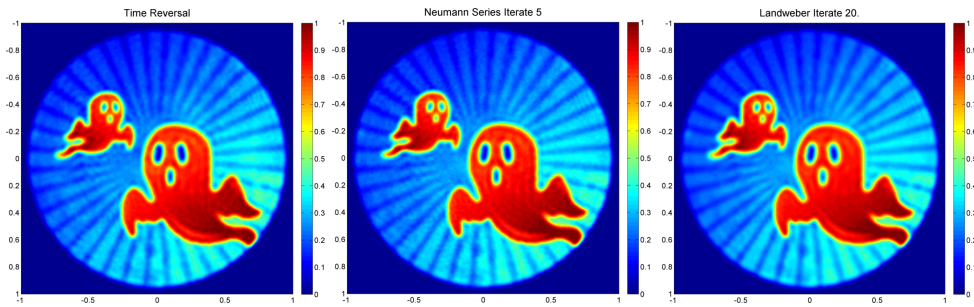


Figure 3: Data: Non-trapping speed, $T = 4T_0$.

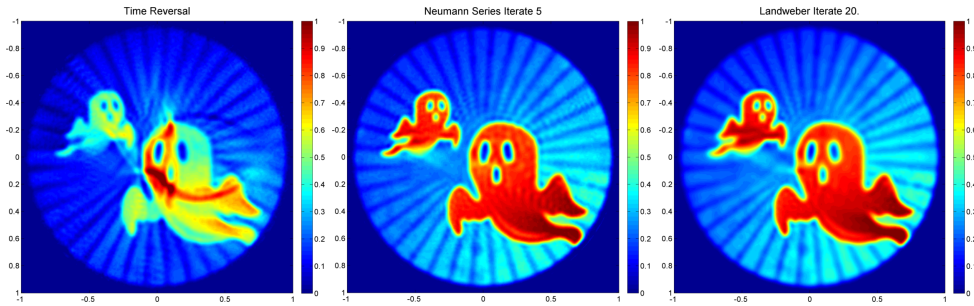


Figure 4: Data: Non-trapping speed, $T = 1.2T_0$.

therefore are interested in the case where the measurement time is shorter, e.g. T as near as possible at T_0 . In Figure 4 we compare the time reversal reconstruction and the Neumann series approach with our method, using $T = 1.2T_0$. The Landweber reconstruction is stopped at a suitable stage of iteration. In practice, the improvement is very large in the first steps, while it needs a lot of iterations to satisfy the discrepancy principle from Theorem 2.2.

The main differences are clearly visible to the naked eye: The time reversal reconstruction fails to compute the central point in the image and produces artifacts. These artifacts can be avoided by the use of the harmonic extension as in (24). We here present iterate $j = 5$ of the Neumann series (28). Also the Landweber reconstruction avoids to amplify the artifacts in the image center. Moreover, it delivers the correct quantitative values of the initial pressure, whereas time reversal underestimates these

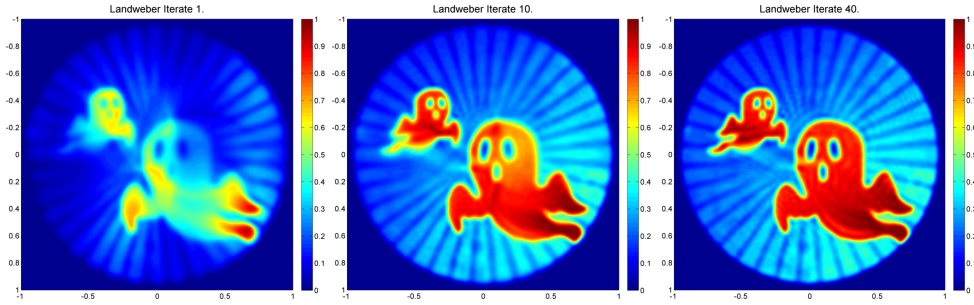
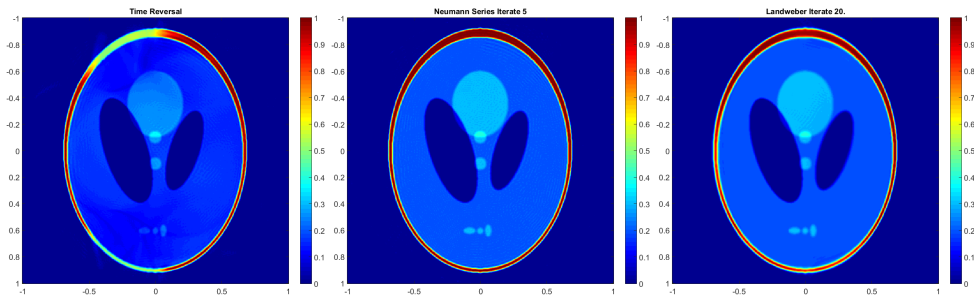


Figure 5: Landweber reconstruction at different iterations. Data: Non-trapping speed, $T = 1.2T_0$.



values. However, the smoothing step naturally included in every Landweber iteration seems to make this approach more stable than the time reversal Neumann series. In fact, at least with our method of numerical wave propagation, we have to stop the Neumann series after 5-10 iterates before numerical errors are amplified too much.

Remark 4.1 (Convergence rates in practice) *The main difference between the convergence rates of the Neumann series and the Landweber iteration lies in the division by c^2 after every backpropagation step, indicated by (15).*

In Figure 5 we show reconstructions using the non-trapping speed and measurement time $T = 1.2T_0$. The measured error $\|y^\delta - Lf_k\|_{L^2(\Sigma)}$ keeps decreasing till $k = 50$. However, the major visible improvements seem to occur within the first 20 iterations. We therefore use the picture of iteration number 20 for our practical comparisons with the other methods.

4.2 Trapping sound speed

In the second example, we want to deal with the trapping speed

$$c(x) = \begin{cases} 1 + 0.5 \sin(-3\pi x_1) \cos(3\pi x), & x \in B_{R-\varepsilon}, \\ 1 & \text{outside } B_R. \end{cases}$$

In this case, there are geodesics present that do not propagate singularities to the measurement surface within finite time. The Landweber approach is the only one that gives a theoretical convergence result in this case. In practice, we see that conventional time reversal, at least for $T = 1.2T_0$, fails to give a detailed reconstruction. The Neumann series approach and the Landweber iteration behave similarly, again with

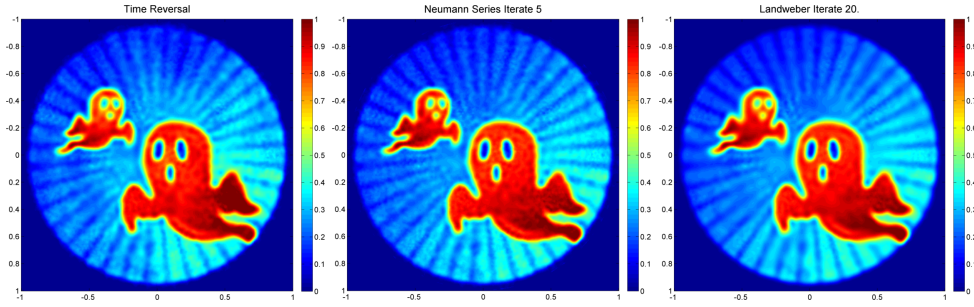


Figure 6: Data: Trapping speed, $T = 4T_0$.

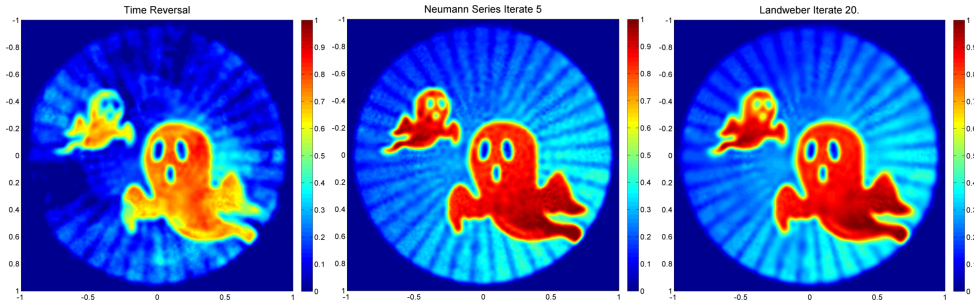


Figure 7: Data: Trapping speed, $T = 2T_0$.

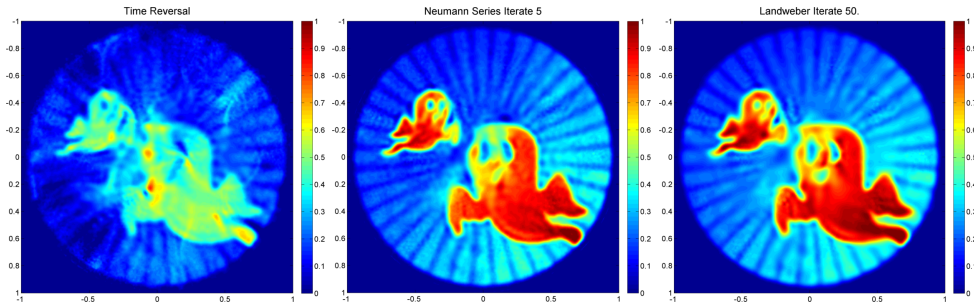


Figure 8: Data: Trapping speed, $T = 1.2T_0$.

the advantage of the Neumann series giving faster convergence, whereas the Landweber gives a regularized solution that seems to be more robust against numerical errors and noise (figures 6, 7 and 8).

Acknowledgement

The work of TG and OS is supported by the Austrian Science Fund (FWF), Project P26687-N25 Interdisciplinary Coupled Physics Imaging.

References

- [1] T. Abboud, P. Joly, J. Rodriguez and I. Terrasse. Coupling discontinuous Galerkin methods and retarded potentials for transient wave propagation on unbounded domains. *J. Comput. Phys.*, 230(15):5877–5907, 2011.
- [2] R. A. Adams. *Sobolev Spaces*. Academic Press, New York, 1975.
- [3] M. Agranovsky and P. Kuchment. Uniqueness of reconstruction and an inversion procedure for thermoacoustic and photoacoustic tomography with variable sound speed. *Inverse Probl.*, 23(5):2089–2102, 2007.
- [4] C. Bardos, G. Lebeau and J. Rauch. Sharp sufficient conditions for the observation, control, and stabilization of waves from the boundary. *SIAM J. Control Optim.* 30(5): 1024–1065, 1992.
- [5] B. Cockburn. Discontinuous Galerkin methods. *ZAMM Z. Angew. Math. Mech.*, 83(11):731–754, 2003.
- [6] G. Cohen, P. Joly, J. E. Roberts and N. Tordjman Higher order triangular finite elements with mass lumping for the wave equation. *SIAM J. Num. An.* 38(6): 2047–2078, 2001.
- [7] D. Colton and R. Kress. *Inverse acoustic and electromagnetic scattering theory*, volume 93 of *Applied Mathematical Sciences*. Springer-Verlag, Berlin, 1992.
- [8] Y. Dong, T. Görner, and S. Kunis. An algorithm for total variation regularized photoacoustic imaging. *Adv. Comput. Math.*, 41(2):423–438, 2014.
- [9] H. W. Engl, M. Hanke, and A. Neubauer. *Regularization of inverse problems*, volume 375 of *Mathematics and its Applications*. Kluwer Academic Publishers Group, Dordrecht, 1996.
- [10] L. C. Evans. *Partial Differential Equations*, volume 19 of *Graduate Studies in Mathematics*. American Mathematical Society, Providence, RI, 1998.
- [11] S. Falletta and G. Monegato. An exact non reflecting boundary condition for 2D time-dependent wave equation problems. *Wave Motion* 51 (2014) 168–192.
- [12] S. Falletta, G. Monegato, and L. Scuderi. A space-time bie method for nonhomogeneous exterior wave equation problems. the Dirichlet case. *IMA J. Numer. Anal.*, 32(1), January 2012.
- [13] M. Fink. Time reversal of ultrasonic fields. i. basic principles. *IEEE Trans. Ultrason., Ferroelectr., Freq. Control*, 39(5):555–566, 1992.
- [14] F. G. Friedlander. *The wave equation on a curved space-time*. Cambridge University Press, Cambridge, UK, 1975.
- [15] C. W. Groetsch. *The theory of Tikhonov regularization for Fredholm Equations of the first kind*. Pitman, Boston, 1984.
- [16] H. Grün, C. Hofer, M. Haltmeier, G. Paltauf, and P. Burgholzer. Thermoacoustic imaging using time reversal. In *Proceedings of the International Congress on Ultrasonics*, pp. 1–4, 2007. paper ID 1542.

- [17] H. Grün, G. Paltauf, M. Haltmeier, and P. Burgholzer. Photoacoustic tomography using a fiber based Fabry-Perot interferometer as an integrating line detector and image reconstruction by model-based time reversal method. In C. D. Depeursinge, editor, *Novel Optical Instrumentation for Biomedical Applications III*, volume 6631 of *Proceedings of SPIE*, page 663107. SPIE, 2007.
- [18] T. Ha-Duong. On retarded potential boundary integral equations and their discretisation. In *Topics in computational wave propagation: Direct and Inverse Problems*, Lecture notes in computational science and engineering, pages 301–336. Springer, Berlin-Heidelberg, 2003.
- [19] M. Hanke. *Conjugate Gradient Type Methods for Ill-Posed Problems*, volume 327 of *Pitman Research Notes in Mathematics Series*. Longman Scientific & Technical, Harlow, 1995.
- [20] Y. Hristova. Time reversal in Thermoacoustic tomography—an error estimate. *Inverse Probl.*, 25(5):055008 (14pp), 2009.
- [21] Y. Hristova, P. Kuchment, and L. Nguyen. Reconstruction and time reversal in Thermoacoustic tomography in acoustically homogeneous and inhomogeneous media. *Inverse Problems*, 24(5):055006 (25pp), 2008.
- [22] A. Kirsch. *An introduction to the mathematical theory of inverse problems*, volume 120 of *Applied Mathematical Sciences*. Springer-Verlag, New York, 2 edition, 2011.
- [23] V. Komornik. *Exact controllability and stabilization; the multiplier method*. *Res. Appl. Math.*, Wiley-Masson, Paris, 1994.
- [24] P. Kuchment and L. A. Kunyansky. Mathematics of Thermoacoustic and Photoacoustic tomography. *European J. Appl. Math.*, 19:191–224, 2008.
- [25] P. Kuchment and L. Kunyansky. Mathematics of photoacoustic and thermoacoustic tomography. In O. Scherzer, editor, [34], pages 817–867. Springer, 2011.
- [26] L. Kunyansky. Reconstruction of a function from its spherical (circular) means with the centers lying on the surface of certain polygons and polyhedra. *Inverse Probl.*, 27(2):025012, 2011.
- [27] J.-L. Lions. Contrôlabilité exacte, perturbations et stabilisation de systèmes distribués. *Tome 1, Vol. 8 of Recherches en Mathématiques Appliquées -Research in Applied Mathematics-*. Masson, Paris, 1988.
- [28] J.-L. Lions and E. Magenes. Non-homogeneous boundary value problems and applications II, *Springer Verlag*, New York, 1972.
- [29] C. Lubich. Convolution quadrature and discretized operational calculus. i. *Numer. Math.*, 52:129–145, 1988.
- [30] D. Modgil, M. A. Anastasio, and P. J. Rivière. Image reconstruction in photoacoustic tomography with variable speed of sound using a higher-order geometrical acoustics approximation. *J. Biomed. Opt.*, 15(2):021308, 2010.
- [31] M.Z. Nashed, editor. *Generalized inverses and applications*. Academic Press [Harcourt Brace Jovanovich Publishers], New York, 1976.

- [32] J. Qia, P. Stefanov, G. Uhlmann, and H. Zhao. An efficient Neumann series-based algorithm for thermoacoustic and photoacoustic tomography with variable sound speed. *SIAM J. Imaging Sciences*, 4(3):850–883, 2011.
- [33] O. Scherzer, M. Grasmair, H. Grossauer, M. Haltmeier, and F. Lenzen. *Variational methods in imaging*. Number 167 in Applied Mathematical Sciences. Springer, New York, 2009.
- [34] O. Scherzer, editor. *Handbook of Mathematical Methods in Imaging*. Springer, New York, 2011.
- [35] P. Stefanov and G. Uhlmann. Thermoacoustic tomography with variable sound speed. *Inverse Probl.*, 25(7):075011, 16, 2009.
- [36] P. Stefanov and G. Uhlmann. Thermoacoustic tomography arising in brain imaging. *Inverse Probl.*, 27(4):045004, 26, 2011.
- [37] B. E. Treeby and B. T. Cox. K-Wave: MATLAB toolbox for the simulation and reconstruction of photoacoustic wave fields. *J. Biomed. Opt.*, 15(2):021314, 2010.
- [38] K. Wang and M. A. Anastasio. Photoacoustic and thermoacoustic tomography: image formation principles. In O. Scherzer, editor, [34], pages 781–817. Springer, 2011.
- [39] L. V. Wang. Prospects of photoacoustic tomography. *Med. Phys.*, 35(12):5758–5767, 2008.
- [40] L. V. Wang, editor. *Photoacoustic imaging and Spectroscopy*. Optical Science and Engineering. CRC Press, Boca Raton, 2009.
- [41] M. Xu and L. V. Wang. Exact frequency-domain reconstruction for Thermoacoustic tomography–I: Planar geometry. *IEEE Trans. Med. Imag.*, 21:823–828, 2002.
- [42] M. Xu and L. V. Wang. Time-domain reconstruction for Thermoacoustic tomography in a spherical geometry. *IEEE Trans. Med. Imag.*, 21(7):814–822, 2002.
- [43] M. Xu and L. V. Wang. Photoacoustic imaging in biomedicine. *Rev. Sci. Instruments*, 77(4):1–22, 2006. Article ID 041101.
- [44] M. Xu, Y. Xu, and L. V. Wang. Time-domain reconstruction algorithms and numerical simulations for Thermoacoustic tomography in various geometries. *IEEE Trans. Biomed. Eng.*, 50(9):1086–1099, 2003.
- [45] Y. Xu, D. Feng, and L. V. Wang. Exact frequency-domain reconstruction for Thermoacoustic tomography–I: Planar geometry. *IEEE Trans. Med. Imag.*, 21(7):823–828, 2002.
- [46] Y. Xu, M. Xu, and L. V. Wang. Exact frequency-domain reconstruction for Thermoacoustic tomography–II: Cylindrical geometry. *IEEE Trans. Med. Imag.*, 21:829–833, 2002.
- [47] Y. Zhang, Y. Wang, and C. Zhang. Total variation based gradient descent algorithm for sparse-view photoacoustic image reconstruction. *Ultrasonics*, 52:1046–1055, 2012.

Appendices

A Well-posedness of the transmission problem

Notation 3 • *The space*

$$V := \{u \in H_0^1(\mathbb{R}^n) : u|_\Omega \in H^1(\Omega)\} \quad (41)$$

is a Hilbert space with respect to the inner product

$$\langle \phi_1, \phi_2 \rangle_V = \int_\Omega \phi_1(x)\phi_2(x) dx + \int_{\mathbb{R}^n} \nabla \phi_1 \cdot \nabla \phi_2 dx .$$

The completeness follows directly from the properties of the Sobolev spaces $H_0^1(\mathbb{R}^n)$ and $H^1(\Omega)$.

The dual space is denoted by V' .

•

Definition A.1 *For $h \in C^\infty((0, T) \times \partial\Omega)$. A weak solution z of (16) satisfies:*

•

$$z \in L^2(0, T; V), z' \in L^2(0, T; L^2(\mathbb{R}^n)), z'' \in L^2(0, T; V'),$$

where V is defined in (41), together with

- $z(T) = z'(T) = 0$. Note that and thus $z \in H^1(0, T; L^2(\mathbb{R}^n))$ and $z' \in H^1(0, T; V')$, such that the traces make sense. In fact $z(T) \in L^2(\mathbb{R}^n)$ and $z'(T) \in V'$.

•

$$\begin{aligned} & \int_0^T \int_{\mathbb{R}^n} \frac{1}{c^2} z'' v dx dt + \int_0^T \int_{\mathbb{R}^n} \nabla z(t) \cdot \nabla v(t) dx dt \\ &= - \int_0^T \int_{\partial\Omega} h(t)v(t) dS(x) dt , \quad \text{for all } v \in L^2(0, T; V). \end{aligned} \quad (42)$$

Note, that the definition of a weak solution is not used consistently in the literature. Evans [10], for instance, uses the test functions v time independently, and formulates a weak form of (16) for almost all $t \in (0, T)$.

Theorem A.2 *For $h \in C^\infty((0, T) \times \partial\Omega)$ there exists a weak solution z of (16) - that is of (42).*

Proof. The proof is similar to [10, Section 7.2.2].

1. First we construct a Galerkin-approximation: Let $\{w_k\}_{k=1}^\infty$ be an orthonormal basis of $L^2(\mathbb{R}^n)$, which is an orthogonal basis for $H_0^1(\mathbb{R}^n)$. For fixed m let

$$z_m(t) = \sum_{k=1}^m d_m^k(t) w_k, \quad t \in (0, T),$$

where

$$d_m^k(T) = 0, d_m^{k'}(T) = 0 \text{ meaning that } z_m(T) = z_m'(T) = 0. \quad (43)$$

and

$$\left\langle \frac{z_m''}{c^2}, w_k \right\rangle_{L^2(\mathbf{R}^n)} + \langle z_m, w_k \rangle_{H_0^1(\mathbf{R}^n)} = \langle h, w_k \rangle_{L^2(\Sigma)}, \quad (44)$$

for all $0 < t < T$, for all $k = 1, \dots, m$.

Analogously to [10, Theorem 1, Section 7.2.2] the Galerkin approximation can be shown.

2. The following estimates are different to [10, Theorem 1, Section 7.2.2] and thus included - it is essential to consider an additional time integration. As in [10] we use $z_m'(t) = \sum_{k=1}^m d_m^k(t) w_k$ as a test function in the Galerkin approximation. However, we do not apply it pointwise for every $\tau \in (0, T)$, but in integrated form. Then from (44) it follows that

$$\int_{\tau}^T \int_{\mathbf{R}^n} \frac{z_m''(\hat{t})}{c^2} z_m'(\hat{t}) + \nabla z_m \cdot \nabla z_m' dx d\hat{t} = - \int_{\partial\Omega} \int_{\tau}^T h(\hat{t}) z_m'(\hat{t}) d\hat{t} dS(x) \\ \text{for all } \tau \in (0, T).$$

Partial integration of the right hand side and evaluation of the integral terms on the left hand gives

$$\int_{\tau}^T \frac{d}{d\hat{t}} \left(\left\| \frac{z_m'(\hat{t})}{c^2} \right\|_{L^2(\mathbf{R}^n)}^2 + \|z_m(\hat{t})\|_{H_0^1(\mathbf{R}^n)}^2 \right) d\hat{t} \\ = 2 \left(\int_{\partial\Omega} \int_{\tau}^T h'(\hat{t}) z_m(\hat{t}) d\hat{t} dS(x) - \int_{\partial\Omega} h(\tau) z_m(\tau) dS(x) \right). \quad (45)$$

Since $z_m(T) = z_m'(T) = 0$, the left hand side equals

$$-(\|z_m'(\tau)\|_{L^2(\mathbf{R}^n)}^2 + \|z_m(\tau)\|_{H_0^1(\mathbf{R}^n)}^2).$$

Estimating the right hand side by Cauchy-Schwarz-inequality and using mean inequality, we get for an arbitrary $D > 0$:

$$\left\| \frac{z_m'(\tau)}{c^2} \right\|_{L^2(\mathbf{R}^n)}^2 + \|z_m(\tau)\|_{H_0^1(\mathbf{R}^n)}^2 \\ \leq \frac{1}{D^2} \left(\int_{\tau}^T \|h'(\hat{t})\|_{L^2(\partial\Omega)}^2 d\hat{t} + \|h(\tau)\|_{L^2(\partial\Omega)}^2 \right) \\ + D^2 \left(\int_{\tau}^T \|z_m(\hat{t})\|_{L^2(\partial\Omega)}^2 d\hat{t} + \|z_m(\tau)\|_{L^2(\partial\Omega)}^2 \right).$$

Let

$$\mathcal{C}(h, \tau) := \int_{\tau}^T \|h'(\hat{t})\|_{L^2(\partial\Omega)}^2 d\hat{t} + \|h(\tau)\|_{L^2(\partial\Omega)}^2, \\ \hat{\mathcal{C}}(h, t) := \int_t^T \mathcal{C}(h, \tau) \tau,$$

and using the trace theorem (4) it follows that

$$\left\| \frac{z_m'(\tau)}{c^2} \right\|_{L^2(\mathbf{R}^n)}^2 + \|z_m(\tau)\|_{H_0^1(\mathbf{R}^n)}^2 \\ \leq \frac{1}{D^2} \mathcal{C}(h, \tau) + D^2 C_{\gamma}^2 \left(\int_{\tau}^T \|z_m(\hat{t})\|_{H^1(\Omega)}^2 d\hat{t} + \|z_m(\tau)\|_{H^1(\Omega)}^2 \right).$$

By integrating of τ over $[t, T]$ we get the following estimate for all $t \in (0, T)$:

$$\begin{aligned} & \int_t^T \left\| \frac{z'_m(\tau)}{c^2} \right\|_{L^2(\mathbf{R}^n)}^2 + \|z_m(\tau)\|_{H_0^1(\mathbf{R}^n)}^2 d\tau \\ & \leq \frac{1}{D^2} \hat{\mathcal{C}}(h, t) + D^2 C_\gamma^2 \int_t^T \left(\int_\tau^T \|z_m(\hat{t})\|_{H^1(\Omega)}^2 d\hat{t} + \|z_m(\tau)\|_{H^1(\Omega)}^2 \right) d\tau. \end{aligned} \quad (46)$$

In addition, because $z_m(T) = 0$, we know that

$$\begin{aligned} \left(\int_\Omega z_m(\tau) dx \right)^2 &= \left(\int_\Omega z_m(\tau) - z_m(T) dx \right)^2 \\ &= \left(\int_\tau^T \int_\Omega z'_m(\hat{t}) dx d\hat{t} \right)^2 \\ &\leq T \int_\tau^T \int_\Omega \left(\frac{z'_m(\hat{t})}{c^2} \right)^2 dx d\hat{t} \\ &= T \int_\tau^T \left\| \frac{z'_m(\hat{t})}{c^2} \right\|_{L^2(\mathbf{R}^n)}^2 d\hat{t}. \end{aligned} \quad (47)$$

Moreover, we know from the inequality from that

$$\left\| z_m(\tau) - \int_\Omega z_m(\tau) dx \right\|_{L^2(\Omega)} \leq C_G \|z_m(\tau)\|_{H_0^1(\mathbf{R}^n)},$$

which implies that for all $\tau \in (0, T)$:

$$\|z_m(\tau)\|_{L^2(\Omega)}^2 \leq \left(\int_\Omega z_m(\tau) dx \right)^2 + 2C_G^2 \|z_m(\tau)\|_{H_0^1(\mathbf{R}^n)}^2,$$

and consequently

$$\|z_m(\tau)\|_{H^1(\Omega)}^2 \leq \left(\int_\Omega z_m(\tau) dx \right)^2 + (2C_G^2 + 1) \|z_m(\tau)\|_{H_0^1(\mathbf{R}^n)}^2.$$

Thus it follows from (46) that

$$\begin{aligned} & \int_t^T \left\| \frac{z'_m(\tau)}{c^2} \right\|_{L^2(\mathbf{R}^n)}^2 + \|z_m(\tau)\|_{H_0^1(\mathbf{R}^n)}^2 d\tau \\ & \leq \frac{1}{D^2} \hat{\mathcal{C}}(h, t) \\ & \quad + D^2 C_\gamma^2 (2C_G + 1) \int_t^T \left(\int_\tau^T \|z_m(\hat{t})\|_{H_0^1(\mathbf{R}^n)}^2 d\hat{t} + \|z_m(\tau)\|_{H_0^1(\mathbf{R}^n)}^2 \right) d\tau \\ & \quad + \int_0^T \left(\int_\Omega z_m(\tau) dx \right)^2 d\tau. \end{aligned} \quad (48)$$

Taking $t = 0$ then gives

$$\begin{aligned}
& \int_0^T \left\| \frac{z'_m(\tau)}{c^2} \right\|_{L^2(\mathbf{R}^n)}^2 + \|z_m(\tau)\|_{H_0^1(\mathbf{R}^n)}^2 d\tau \\
& \leq \frac{1}{D^2} \hat{\mathcal{C}}(h, t) \\
& \quad + D^2 C_\gamma^2 (2C_G + 1)(T + 1) \int_0^T \|z_m(\hat{t})\|_{H_0^1(\mathbf{R}^n)}^2 d\hat{t} \\
& \quad + \int_0^T \left(\int_\Omega z_m(\tau) dx \right)^2 d\tau .
\end{aligned} \tag{49}$$

Thus it follows from (47) that

$$\begin{aligned}
& \frac{1}{2T} \int_0^T \left(\int_\Omega z_m(\tau) dx \right)^2 d\tau + \\
& \quad \frac{1}{2} \int_0^T \left\| \frac{z'_m(\tau)}{c^2} \right\|_{L^2(\mathbf{R}^n)}^2 + \|z_m(\tau)\|_{H_0^1(\mathbf{R}^n)}^2 d\tau \\
& \leq \frac{1}{D^2} \hat{\mathcal{C}}(h, t) \\
& \quad + D^2 C_\gamma^2 (2C_G + 1)(T + 1) \int_0^T \|z_m(\hat{t})\|_{H_0^1(\mathbf{R}^n)}^2 d\hat{t} \\
& \quad + \int_0^T \left(\int_\Omega z_m(\tau) dx \right)^2 d\tau .
\end{aligned}$$

Choosing D such that

$$\max \{ D^2 C_\gamma^2 (2C_G + 1)(T + 1), 2D^2 C_\gamma^2 (T + 1) \} \leq \frac{1}{2},$$

provides that

$$\begin{aligned}
& \frac{1}{4T} \int_0^T \left(\int_\Omega z_m(\tau) dx \right)^2 d\tau + \\
& \quad \frac{1}{4} \int_0^T \left\| \frac{z'_m(\tau)}{c^2} \right\|_{L^2(\mathbf{R}^n)}^2 + \|z_m(\tau)\|_{H_0^1(\mathbf{R}^n)}^2 d\tau \\
& \leq \frac{1}{D^2} \hat{\mathcal{C}}(h, t) .
\end{aligned} \tag{50}$$

Therefore there exists a constant \mathcal{C} such that

$$\max \left\{ \|z'_m\|_{L^2(0, T; \mathbf{R}^n)}, \|z_m\|_{L^2(0, T; H_0^1(\mathbf{R}^n))}, \|z_m|_\Omega\|_{L^2(0, T; H^1(\Omega))} \right\} \leq \mathcal{C}, \tag{51}$$

where the last estimate is again due to inequality , already used above.

Because $\{w_k\}$ is a basis it follows from (44) that for all $v \in L^2(0, T; V)$:

$$\sup_v \left\langle \frac{z''_m}{c^2}, v \right\rangle_{L^2(0, T; \mathbf{R}^n)} \leq \sup_v \langle z_m, v \rangle_{H_0^1(0, T; \mathbf{R}^n)} + \sup_v \langle h, v \rangle_{L^2(\Sigma)} \leq C(h, \mathcal{C}),$$

where $C(h, \mathcal{C})$ is constant depending on h and \mathcal{C} , but is not dependent on m . This shows that $\in L^2(0, T; V')$.

3. (50) guarantees that $\{z_m\}$ is uniformly bounded in $L^2(0, T; H_0^1(\mathbb{R}^n))$, and $\{z_m|_\Omega\}$ is uniformly bounded in $L^2(0, T; H^1(\Omega))$. Moreover, $\{z'_m\}$ is uniformly bounded in $L^2(0, T; L^2(\mathbb{R}^n))$, and $\{z''_m\}$ is uniformly bounded in $L^2(0, T; V')$. Thus it has a weakly convergent subsequence, which we again denote by $\{z_m\}$ which is converging weakly in the following sense:

$$\begin{aligned} \{z_m\} &\rightharpoonup z \text{ with respect to } L^2(0, T; H_0^1(\mathbb{R}^n)), \\ \{z_m|_\Omega\} &\rightharpoonup z|_\Omega \text{ with respect to } L^2(0, T; H^1(\Omega)), \\ \{z'_m\} &\rightharpoonup \psi \text{ with respect to } L^2(0, T; L^2(\mathbb{R}^n)), \\ \{z''_m\} &\rightharpoonup \rho \text{ with respect to } L^2(0, T; V'). \end{aligned}$$

We note that the trace operator $\gamma : H^1(\Omega) \rightarrow L^2(\partial\Omega)$ is bounded. Therefore, every test function $v \in L^2(0, T; V)$ satisfies $v|_{\partial\Omega} \in L^2(0, T; L^2(\partial\Omega))$. Consequently,

$$\int_0^T \int_{\partial\Omega} z_m v \, dS(x), dt \rightarrow \int_0^T \int_{\partial\Omega} z v \, dS(x), dt.$$

Now, let $v \in C_0^\infty((0, T) \times \mathbb{R}^n)$, then $v', v'' \in C_0^\infty((0, T) \times \mathbb{R}^n)$ as well, such that

$$\begin{aligned} \int_0^T \int_\Omega \psi v \, dx dt &= \lim \int_0^T \int_\Omega z'_m v \, dx dt \\ &= - \lim \int_0^T \int_\Omega z_m v' \, dx dt \\ &= \lim \int_0^T \int_\Omega z v' \, dx dt \\ &= \lim \int_0^T \int_\Omega z' v \, dx dt, \end{aligned}$$

which implies that $\psi = z'$. Analogously one can show that $z''_m \rightarrow z''$ in $L^2(0, T; V')$. Therefore, z it is a solution of (42). □

Theorem A.3 *The solution of (16) is unique in $L^2(0, T; V)$.*

Proof. Let us assume that there exist two solutions z_1, z_2 of (16). Then

$$\begin{aligned} \frac{1}{c^2} (z_1 - z_2)'' - \Delta(z_1 - z_2) &= 0 \text{ in } \mathbb{R}^n \setminus \partial\Omega \times (0, T), \\ (z_1 - z_2)(T) = (z_1 - z_2)'(T) &= 0 \text{ in } \mathbb{R}^n, \\ [(z_1 - z_2)] = 0, \quad \left[\frac{\partial(z_1 - z_2)}{\partial \mathbf{n}} \right] &= 0 \text{ on } \partial\Omega \times (0, T). \end{aligned} \tag{52}$$

But this solution has only a trivial solution, which one sees from (7) and by noting the boundary conditions at ∞ of an $H_0^1(\mathbb{R}^n)$ function. □